THE JOURNAL OF PHYSICAL CHEMISTRY C

Article

pubs.acs.org/JPCC

Optimization of $PbI_2/MAPbI_3$ Perovskite Composites by Scanning Electrochemical Microscopy

Hsien-Yi Hsu,[†,§] Li Ji,[†,‡,§] Minshu Du,[†] Ji Zhao,[†] Edward T. Yu,[‡] and Allen J. Bard*[,†]

[†]Center for Electrochemistry, Department of Chemistry, The University of Texas at Austin, Austin, Texas 78712, United States

[‡]Microelectronics Research Center, Department of Electrical and Computer Engineering, University of Texas at Austin, Austin, Texas 78712, United States

Supporting Information

ABSTRACT: A variety of $PbI_2/MAPbI_3$ perovskites were prepared and investigated by a rapid screening technique utilizing a modified scanning electrochemical microscope (SECM) in order to determine how excess PbI_2 affects its photoelectrochemical (PEC) properties. An optimum ratio of 2.5% $PbI_2/MAPbI_3$ was found to enhance photocurrent over pristine $MAPbI_3$ on a spot array electrode under irradiation. With bulk films of various $PbI_2/MAPbI_3$ composites prepared by a spin-coating technique of mixed precursors and a one-step annealing process, the 2.5% $PbI_2/MAPbI_3$ produced an increased photocurrent density compared to pristine $MAPbI_3$ for 2 mM benzoquinone (BQ) reduction at −0.4 V vs Fc/Fc^+. As a result of the relatively high quantum yield of $MAPbI_3$, a time-resolved photoluminescence quenching experiment could be applied to determine electron−hole diffusion coefficients and diffusion lengths of $PbI_2/MAPbI_3$ composites, respectively. The diffusion coefficients combined with the exciton lifetime of the pristine 2.5% $PbI_2/MAPbI_3$ (τ_{PL} = 103.3 ns) give the electron and hole exciton diffusion lengths, ∼300 nm. Thus, the 2.5% $PbI_2/MAPbI_3$ led to an approximately 3.0-fold increase in the diffusion length compared to a previous report of ∼100 nm for the pristine $MAPbI_3$ perovskite. We then demonstrated that the efficiency of liquid-junction solar cells for 2.5% excess PbI_2 of p-$MAPbI_3$ was improved from 6.0% to 7.3%.

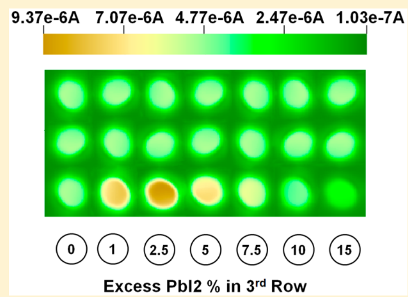

■ INTRODUCTION

Organic−inorganic hybrid lead-based perovskites exhibit remarkable properties, including high absorption coefficients, long exciton lifetimes and diffusion lengths, high charge-carrier mobilities, and low exciton binding energies,[1−4] and have yielded power conversion efficiencies (PCE) of ∼20% in photovoltaic cells.[5−8] These photovoltaic cells usually are titanium dioxide (TiO_2) dye-sensitized solar cells (DSSC)[9,10] and solid-state solar cells.[8,11−17] In a previous paper, we described liquid junction PEC solar cells involving $MAPbI_3$ perovskites.[18] The $MAPbI_3$ perovskites are extremely sensitive to moisture[19] and unstable in polar solvents. However, dichloromethane (CH_2Cl_2) can be used for liquid junction PEC solar cells with reasonable stability because of its relatively higher dielectric constant and is also useful for fundamental studies.[18] More importantly, the use of liquid electrolytes allows easy combinatorial synthesis and screening of new perovskite materials in arrays and testing the effects of various dopants on them. In this article, we describe such studies using robotic synthesis and rapid screening based on scanning electrochemical microscopy (SECM).

$MAPbI_3$ perovskites were synthesized with equimolar mixture of MAI and PbI_2. Dittrich et al. showed excess PbI_2 can be used to passivate perovskite grain boundaries and decrease carrier recombination lifetime for improving the performance of perovskite-based solar cells.[20] Burda et al. then confirmed this passivation effect of excess PbI_2 by femtosecond time-resolved transient absorption spectroscopy (fs-TA) of $MAPbI_3$ perovskite films.[21] The peak intensities of perovskite TA were used to estimate relative amounts of excess PbI_2 in the samples, while powder X-ray diffraction (XRD) can independently confirm the existence of excess PbI_2. Time-resolved transient absorption demonstrated that perovskite films with less excess PbI_2 displayed faster relaxation rates. These fast dynamics are assigned to charge carrier trapping at perovskite grain boundaries, and the slower dynamics in samples containing PbI_2 are attributed to a passivation effect.[22] However, these studies did not show the amount of PbI_2 required for optimal passivation. Here, our contribution is to screen different quantitative combinations of PbI_2 and $MAPbI_3$ perovskites efficiently by utilizing SECM imaging.

■ EXPERIMENTAL SECTION

Materials. Methylamine (CH_3NH_2, 2 M in methanol, Alfa Aesar), hydroiodic acid (HI, 57 wt % in water, Alfa Aesar), lead iodide (PbI_2, 99.9985% metals basis, Alfa Aesar), *N*,*N*-dimethylformamide (DMF, ≥99.9%, Sigma-Aldrich), methylene chloride (CH_2Cl_2, anhydrous, ≥99.9%, Sigma-Aldrich), tetrahydrofuran (THF, anhydrous, ≥99.9%, Sigma-Aldrich), ethyl acetate (EA, anhydrous, ≥99.8%, Sigma-Aldrich), *p*-benzoquinone (BQ, ≥99.5%, Sigma-Aldrich), tetrabutylammonium

Received: August 3, 2016
Revised: August 4, 2016
Published: August 9, 2016

DOI: 10.1021/acs.jpcc.6b07850
J. Phys. Chem. C 2016, 120, 19890−19895

hexafluorophosphate ($TBAPF_6$, ≥99.9%, Sigma-Aldrich). fluorine doped tin oxide (FTO) coated glass was obtained from Pilkington (Toledo, OH) as a substrate of the electrodes. The 15 × 15 mm squares were cleaned by successive sonication in ethanol and 2-propanol and rinsed with deionized water. Phenyl-C61-butyric acid methyl ester (PCBM; Solenne BV) and 2,2′,7,7′-tetrakis(*N*,*N*-di-*p*-methoxyphenylamine)9,9′-spirobifluorene (spiro-OMeTAD; Borun Chemicals).

Preparation of Perovskite Film. p-$MAPbI_3$ was spin-cast on FTO glass substrates from *N*,*N*-dimethylformamide (DMF) (Alfa Aesar) solution with the mixture of MAI and PbI_2. The weight percent of excess PbI_2 to $MAPbI_3$ was increased in the order of 0%, 1%, 2.5%, 5%, 7.5%, 10%, and 15%. MAI was synthesized by stirring 27.86 mL of methylamine (2 M in methanol, Alfa Aesar) and 30 mL of hydroiodic acid (57 wt % in water, Alfa Aesar) in 250 mL round bottomed flask in an ice bath under an argon atmosphere for 3 h. After the reaction, the solvent was evaporated using a rotary evaporator. A white powder, methylammonium iodide (MAI), was washed with diethyl ether by stirring the solution for 30 min, which was repeated three times and then finally dried at 60 °C in vacuum oven for 24 h.[23] The synthesized MAI white powder was mixed with PbI_2 (Alfa Aesar) in DMF at 100 °C for 1 h.[24] The top quenchers were then deposited in air via spin-coating chlorobenzene solutions with the following conditions: PCBM at 30 mg/mL spin-coated at 1000 rpm and spiro-OMeTAD at 0.46 M spin-coated at 2000 rpm

Preparation of Photocatalyst Spot Array Electrodes. Spot array electrodes (an electrode composed of spots with each spot having a different composition) were fabricated using a previously reported method[25] using a CH Instruments dispenser. The precursor solutions (0.518 M in DMF) were dispensed on the FTO substrate to create the spot array electrode. This was done by moving the piezo-dispensing tip to a programmed position over the FTO substrate and dispensing drops (~100 pL/drop) of the precursor solutions. The PbI_2 precursor solution was dispensed first in a preprogrammed pattern onto the FTO substrate, followed by a second MAI precursor solution dispensed onto the FTO in an overlay pattern. The distance between photocatalyst spots on the array was about 150 μm with a spot diameter of approximately 350 μm. Each spot had a total of 25 drops, and the spot composition is reported as the relative number of drops of each precursor solution. In all cases, the composition of the excess PbI_2 was controlled from 0 to 15 wt % PbI_2-to-$MAPbI_3$ ratio. The prepared arrays were annealed at 100 °C for 1 h in air to form the $MAPbI_3$ perovskites.

Screening the Spot Array Electrodes. A schematic SECM setup has been described previously.[25] Briefly, a 400 μm diameter optical fiber was connected to a 150 W xenon lamp (Oriel) and was attached to the tip holder of a CHI 900B SECM. A 420 nm long-pass filter (removing the UV portion of the spectrum) was used for visible light only illumination in rapid screening experiments. The perovskite array was used as the working electrode and was placed in the bottom of a custom designed Teflon SECM cell with an O-ring (exposed area: 1.0 cm^2). A Pt wire was used as the counter electrode, and a saturated $Ag/AgNO_3$ electrode was used as the reference electrode. The electrolyte consisted of 2 mM BQ and 0.1 M $TBAPF_6$ (supporting electrolyte). Light from the xenon lamp was passed through the optical fiber, positioned perpendicular to the working electrode ~200 μm above the surface, to illuminate one spot on the working electrode at a time. The optical fiber tip was scanned across the spot array electrode with a scan rate of 500 μm/s, while a potential of −0.4 V vs $Ag/AgNO_3$ was applied to the working electrode through the SECM potentiostat. Scanning over the spot arrays revealed two-dimensional images indicative of the generation of photocurrent on each spot.

Photoelectrochemical Measurements. The results on array electrodes were confirmed by PEC of perovskite films. The photoactivity of p-$MAPbI_3$ was measured in a photoelectrochemical cell. The films were used as working electrodes (0.27 cm^2) exposed to electrolyte solution and irradiation. All measurements were carried out in a borosilicate glass cell with a carbon counter electrode and $Ag/AgNO_3$ reference electrode (a silver wire immersed in 0.01 M silver nitrate in MeCN connected to the cell via a 0.10 M $TBAPF_6$ in deaerated CH_2Cl_2 salt bridge).[18] All potentials are reported vs Fc/Fc^+ in deaerated CH_2Cl_2. The light source was irradiated through the electrolyte solution using full output of the Xe lamp with an incident light intensity of about 100 mW/cm^2. The supporting electrolyte was 0.1 M $TBAPF_6$ in deaerated CH_2Cl_2.

Instruments. A CH Instruments Model 760E electrochemical analyzer (Austin, TX) was used as a potentiostat for the experiments with the thin film electrodes. Illumination was with a xenon lamp (XBO 150 W, Osram) at full output for UV−visible irradiation. Glancing incidence angle X-ray diffraction (XRD) measurements were performed by using D8 ADVANCE (Bruker, Fitchburg, WI) equipped with a Cu Kα radiation source where the incident angle was 0.4°. The film thickness was measured by scanning electron microscopy (SEM, Quanta 650 FEG, FEI Company, Inc., Hillsboro, OR). In the solar cell measurements, current (I) and voltage (V) readings were taken between the working electrode and the carbon counter electrode without external power source using a Keithley Model 2400 electrometer and a xenon lamp solar simulator (Newport) equipped with an AM1.5G filter. Emission spectra were obtained by a front-face alignment on a Fluorolog-3 spectrophotometer (Jobin-Yvon) spectrofluorometer. For precursor dispensing, a CH Instruments model 1550 dispenser (Austin, TX) with a piezoelectric dispensing tip (Micro Jet AB-01-60, MicroFab, Plano, TX) connected to an XYZ stage driven by a computer-controlled stepper-motor system (Newport) was used.

■ RESULTS AND DISCUSSION

SECM Scanning of Perovskite Arrays. A method for rapid screening of semiconductor materials using a form of the modified SECM has been described previously.[26] In brief, arrays composed of ~350 μm diameter semiconductor spots with different compositions were deposited by a piezoelectric dispenser onto a conductive fluorine-doped tin oxide (FTO) substrate. The scanning tip of the modified SECM was replaced by a 300 μm fiber optic connected to a xenon lamp and was rapidly scanned over the array. This combinatorial screening technique can reduce the effort and material expended in the optimization process,[27,28] and evaluate the photocurrent response at the substrate of different elements in the semiconductor array.[29] In this study, we performed a rapid screening analysis on $PbI_2/MAPbI_3$ composites with a modified SECM. The arrays contained three rows and seven spots of columns. To test the reproducibility, the first and second seven-spot rows are pristine $MAPbI_3$ perovskites. The photocurrents of all 14 spots are almost the same (~5.6 ± 0.1 μA). The third seven-spot row we analyzed are spot arrays of $MAPbI_3$ perovskite blended with varying excess amounts of the PbI_2 precursor in compositions ranging

DOI: 10.1021/acs.jpcc.6b07850
J. Phys. Chem. C 2016, 120, 19890−19895

from 0 to 15%. Time-resolved photoluminescence spectra on separate films at different concentrations were then monitored for the different ratios of $PbI_2/MAPbI_3$ composites. The SECM imaging and photoluminescence decay kinetics can yield further insight as to which factor primarily affects the resulting enhancement.

While it has been established previously that the maximum photocurrent of photovoltaic devices may be increased by introduction of PbI_2 in $MAPbI_3$,[21] SECM rapid screening of $PbI_2/MAPbI_3$ composite materials enables determination of the optimum amount of PbI_2 in the $MAPbI_3$ perovskite. Employing the SECM technique, we screened spot array electrodes to determine the dependence of photocurrent response on composition of $PbI_2/MAPbI_3$ composites with PbI_2 content ranging from 0 to 15 wt %. The rapid screening results showed that 2.5% of excess PbI_2 to $MAPbI_3$ gave rise to the highest photocurrent improvement under irradiation. When the excess amounts of PbI_2 to $MAPbI_3$ were more than 10%, the photocurrents were lower than that of the pristine $MAPbI_3$. Figure 1 presents a representative example of the SECM result of a $PbI_2/MAPbI_3$ spot array electrode under irradiation. The colors in Figure 1 represent the photocurrent for BQ reduction at an applied potential of −0.4 V vs Fc/Fc^+ with browns representing higher currents and greens representing lower currents. The leftmost spot on the third seven-spot row of the spot array represents pure $MAPbI_3$, and then moving right, each spot has an increased amount of excess PbI_2, as shown by the schematic below the SECM image. At a ratio of 2.5% $PbI_2/MAPbI_3$ spot, the photocurrent was ~9.4 μA, whereas the pure $MAPbI_3$ spot produces a photocurrent of ~5.6 μA.

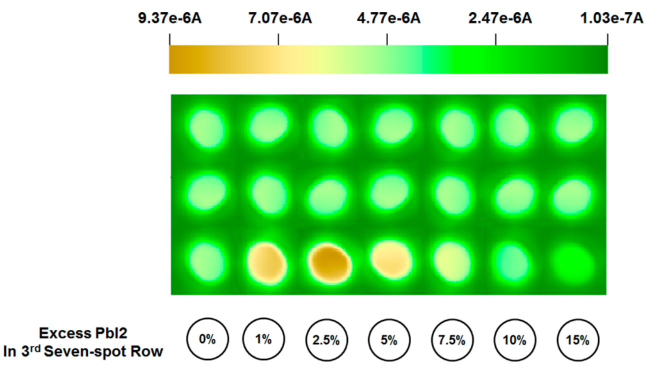

Figure 1. SECM images for a typical photocurrent response of $PbI_2/MAPbI_3$ composites under irradiation. The color represents the measured photocurrent shown in the scale bar above the SECM image. The first and second seven-spot rows are pure $MAPbI_3$ perovskites. The third seven-spot row represents the amount of excess PbI_2 in each spot in the array electrode. The photocurrent shown is for 2 mM BQ reduction with 0.1 M $TBAPF_6$ supporting electrolytes in CH_2Cl_2 measured at an applied potential of −0.4 V vs Fc/Fc^+.

Characterization and Photoelectrochemistry with Thin Bulk Film Samples. A one-step deposition and annealing process made the $MAPbI_3$ perovskite films. Varying the amount of excess PbI_2 in MAI solution made $MAPbI_3$ containing PbI_2. The compositions of $PbI_2/MAPbI_3$ films were characterized by X-ray diffraction (XRD). Without adding excess PbI_2, only the β-phase of the $MAPbI_3$ is formed (Figure 2).[30] PbI_2 can be easily detected by the (001) and (003) reflections at 2θ = 12.56° and 39.42°, respectively.[31] The $MAPbI_3$ thin-film bulk electrodes were then introduced to characterize the PEC performance in order to verify the results of the rapid SECM screening tests. We compared the PEC responses of $MAPbI_3$ to 2.5% $PbI_2/MAPbI_3$ and 15% $PbI_2/MAPbI_3$ for BQ reduction by linear sweep voltammetry (LSV) with chopped light under irradiation (Figure 3). In Figure 3, the LSV was conducted from +0.45 to −0.40 V vs Fc/Fc^+ at a scan rate of 50 mV/s. While the pristine $MAPbI_3$ resulted in a photocurrent of ~4.1 mA/cm^2, the 2.5% and 15% $PbI_2/MAPbI_3$ samples generated a photocurrent of 6.8 and 2.0 mA/cm^2 for BQ reduction, respectively. These results are consistent with those of the SECM screening process illustrated in Figure 1, confirming the validity of the SECM screening technique for determining the dependence of PEC performance on $PbI_2/MAPbI_3$ composite composition.

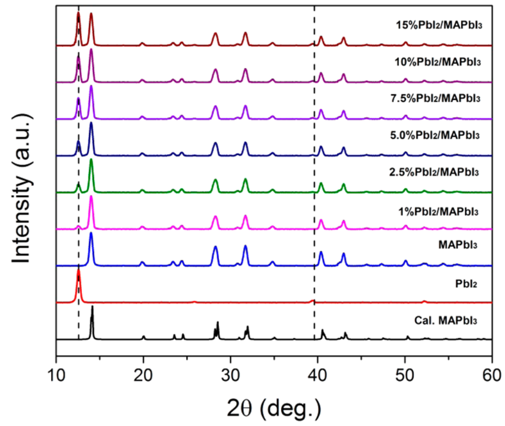

Figure 2. X-ray diffraction patterns of $MAPbI_3$ films with increasing the amount of excess PbI_2.

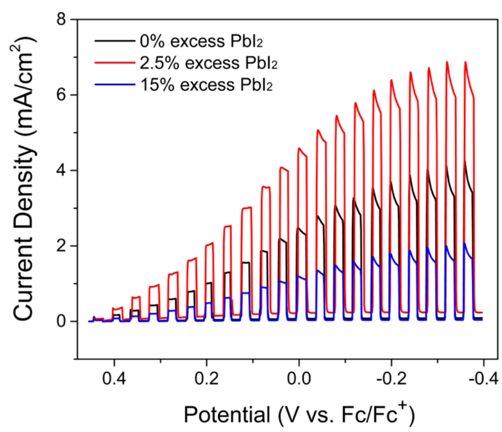

Figure 3. Photoelectrochemical responses of bulk film electrodes, 0% $PbI_2/MAPbI_3$ (black), 2.5% $PbI_2/MAPbI_3$ (red), and 15% $PbI_2/MAPbI_3$ (blue), characterized by linear sweep voltammetry with chopped light under 100 mW/cm^2 irradiation at 50 mV/s. Shown is the photocurrent for BQ reduction in CH_2Cl_2 containing 2 mM BQ and 0.1 M $TBAPF_6$ (supporting electrolyte).

Steady-State Photoluminescence and Photoluminescence Decay Dynamics. Initially the $MAPbI_3$ film samples were prepared including solution preparation and spin coating. The steady-state photoluminescence spectrum for perovskite films was carried out at room temperature under optical excitation with monochromatic laser light at 485 nm, displayed in Figure 4. The photoluminescence of the $MAPbI_3$ films showed a strong band at 770 nm with a full width at half-maximum (fwhm) of 130 nm. Photoluminescence decay dynamics can be applied to determine carrier diffusion parameters in the perovskite

DOI: 10.1021/acs.jpcc.6b07850
J. Phys. Chem. C 2016, 120, 19890−19895

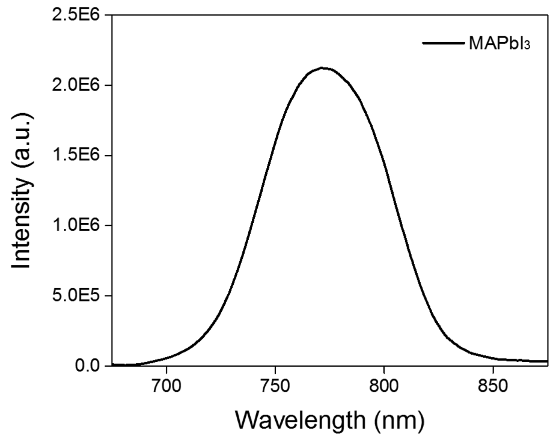

Figure 4. Steady-state photoluminescence spectrum of $MAPbI_3$ film under excitation at 485 nm.

films in the absence and presence of the excess PbI_2.[32] Time-resolved photoluminescence spectra of $MAPbI_3$ perovskite films were then recorded by using a time-correlated single photon counting (TCSPC) system to explore the photoluminescence decay dynamics. Excitation was provided by a 485 nm pulsed laser, which provided <200 ps pulses with the fluence of ~30 nJ/cm^2.[32] The thickness of the $MAPbI_3$ films was approximately 200 nm, which is similar to the typical thickness in photovoltaic devices. The photoluminescence decay at the wavelength of 770 nm was monitored for perovskite films deposited on FTO glass substrates, shown in Figure 5.

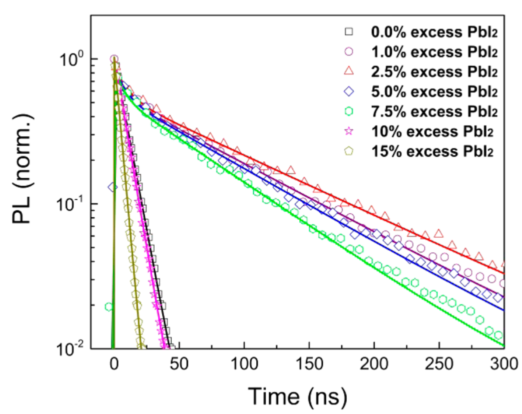

Figure 5. Photoluminescence decay monitored at 770 nm for $PbI_2/MAPbI_3$ composite perovskite films containing 0.0, 1.0, 2.5, 5.0, 7.5, 10, and 15 wt % of excess PbI_2, along with stretched exponential fits. To easily compare lifetimes of all perovskite samples, τ_{PL} are acquired with a biexponential decay function.

The photoluminescence lifetime, τ_{PL}, was determined by fitting exponential functions to the measured decay curves, as shown in Table 1.[32,33] The fitting parameters (τ_1, α_1, τ_2, α_2) and corresponding errors (χ^2) of photoluminescence decay are summarized in Table S1. For the 2.5% $PbI_2/MAPbI_3$, the fast decay component, τ_1, shows a time constant of τ_1 = 9.0 ns, likely due to bimolecular recombination;[34−36] the long decay component τ_2 is assigned to recombination of free carriers in the radiative channel, which matches with the previously reported photoluminescence decay in $MAPbI_3$ films.[32,37] The diffusion lifetime in 2.5% $PbI_2/MAPbI_3$ perovskite films was extended to 103.3 ns because the passivation effect results in the reduction of free carrier recombination. The pristine $MAPbI_3$ film exhibits a time constant of τ_{PL} = 9.10 ns owing to electronic defects at grain boundaries that results in a serious recombination with the relatively lower photocurrent density. In comparison with 2.5% $PbI_2/MAPbI_3$ perovskite films, the long decay component, τ_2, for 5.0% and 7.5% of excess PbI_2 in $MAPbI_3$ film decreased slightly to be 101.6 and 86.7 ns, respectively, because the PbI_2 might become one of the main phases in the perovskite films.[22] By adding 15% of excess PbI_2 in $MAPbI_3$ film, lifetime shortened to a time constant of τ_{PL} = 4.43 ns since higher amount of PbI_2 becomes an insulating layer rather than a passivating layer.[21]

Table 1. Fitted Decay Times (τ_{PL}) and Diffusion Lengths (L_D (e^-) and L_D (h^+) of $PbI_2/MAPbI_3$ Composite Perovskite Films Containing 0.0, 1.0, 2.5, 5.0, 7.5, 10, and 15 wt % of Excess PbI_2

perovskite	τ_{PL} (ns)	L_D (e^-) (nm)	L_D (h^+) (nm)
0% $PbI_2/MeNH_3PbI_3$	9.1 ± 0.1	135	85
1% $PbI_2/MeNH_3PbI_3$	90.7 ± 0.2	301	269
2.5% $PbI_2/MeNH_3PbI_3$	103.3 ± 0.2	321	287
5.0% $PbI_2/MeNH_3PbI_3$	84.6 ± 0.1	291	260
7.5% $PbI_2/MeNH_3PbI_3$	71.3 ± 0.2	267	239
10% $PbI_2/MeNH_3PbI_3$	8.2 ± 0.1	91	81
15% $PbI_2/MeNH_3PbI_3$	4.4 ± 0.1	67	60

The crucial parameters for enhancing the efficiency of photovoltaic devices are the diffusion coefficient and the diffusion length, D and L_D, which can be determined by photoluminescence quenching measurements.[38] By spin-coating either an electron-accepting fullerene [phenyl-C_{61}-butyric acid methyl ester (PCBM)] or a hole-acceptor [2′-7,7′-tetrakis-(*N*,*N*-di-*p*-methoxyphenylamine)-9,9-spirobifluorene (Spiro-OMeTAD)] on top of the perovskite films, quenching samples were fabricated. For the addition of electron and hole-quenchers, PCBM and Spiro-OMeTAD, the lifetimes of $MAPbI_3$/PCBM and $MAPbI_3$/Spiro-OMeTAD were decreased with time constants τ_{PL} of 2.9 ± 0.1 and 4.0 ± 0.1 ns, respectively (Figure S-1). According to a 1-D diffusion model (equation S3, described in detail in Supporting Information),[32] we calculated total decay rate, $k = k_r + k_{nr} = \beta\tau_s^{-\beta}\tau^{\beta-1}$, by using a stretched exponential function to fit photoluminescence decay curves of perovskite films in the absence of any quenchers. The boundary condition $n(L,t) = 0$, where $x = 0$ at the glass/perovskite interface and L is the perovskite film thickness, can be obtained by assuming that all charge carriers that reach the interface are quenched. And then we estimated the electron and hole diffusion coefficients, showing 0.010 ± 0.003 and 0.008 ± 0.002 cm^2/s, respectively. The electron and hole diffusion lengths (L_D) were calculated to be L_D (e^-) = 135 nm and L_D (h^+) = 85 nm by utilizing $L_D = (D\tau_{PL})^{1/2}$, where τ_{PL} is the lifetime in the absence of quenching, tabulated in Table 1. The long transport lengths of $MAPbI_3$ perovskite films are due to its crystal structure containing corner-connected PbI_6 octahedral that form a three-dimensional framework.[12] The diffusion length *I* measured for the pristine $MAPbI_3$ is close to the typical diffusion length for the $MAPbI_3$ perovskite film (~100 nm).[32,37] In comparison to pure $MAPbI_3$, the L_D (e^-) and L_D (h^+) of 2.5% $PbI_2/MAPbI_3$ composites are 321 and 287 nm, which reached about 3.0-fold longer diffusion length than the 0% $PbI_2/MAPbI_3$ sample. We attribute that this result, a reduction in the number of trapping sites, was due to refilling the grain boundaries in the perovskite materials.[22] We then demonstrated that short-circuit current density for 2.5% excess PbI_2 of p-$MAPbI_3$ was increased from 7.8 to 9.8 mA/cm^2, and the efficiency of a liquid-junction

DOI: 10.1021/acs.jpcc.6b07850
J. Phys. Chem. C 2016, 120, 19890−19895

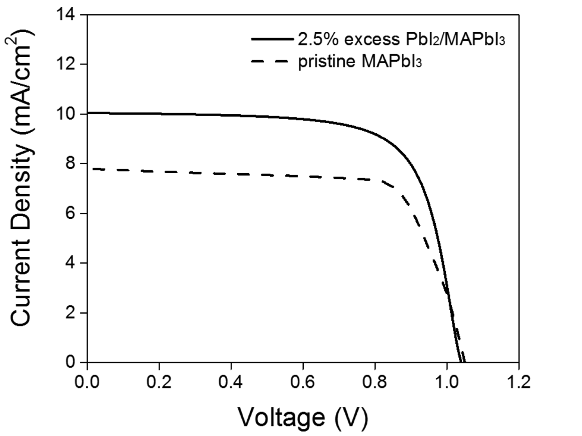

Figure 6. Steady-state current density−voltage relation for perovskite/BQ (2 mM) and $BQ^{\bullet -}$ (2 mM)/C PEC cells under irradiation with a 100 mW/cm^2 xenon lamp focused onto the photoelectrode. The solid curve represents 2.5% excess PbI_2/$MAPbI_3$, and the dashed one is the pristine $MAPbI_3$. The optical path through the solution was about 0.3 mm.

solar cell was improved from 6.0% to 7.3% under irradiation with 100 mW/cm^2, as plotted in Figure 6.

■ SUMMARY AND CONCLUSIONS

We have used a modified SECM imaging apparatus equipped with an optical fiber as a screening tip for determining the optimum amount of excess PbI_2 in $MAPbI_3$-based liquid-junction PEC solar cells. We demonstrate that 2.5% excess PbI_2 of p-$MAPbI_3$ showed stronger photoresponse, higher diffusion length, and longer carrier lifetime in a photoelectrode array system containing excess PbI_2 in p-$MAPbI_3$ perovskite semiconductors on the FTO substrate. The PCE of liquid-junction solar cells was increased to 7.3% as a result of the passivation effect of PbI_2. Hence, the longer diffusion lifetime with less recombination processes leads to higher photocurrent density.

■ ASSOCIATED CONTENT

Ⓢ Supporting Information

The Supporting Information is available free of charge on the ACS Publications website at DOI: 10.1021/acs.jpcc.6b07850.

Time-resolved photoluminescence, diffusion modeling, and parameters of photoluminescence decay (PDF)

■ AUTHOR INFORMATION

Corresponding Author

*E-mail: ajbard@mail.utexas.edu. Phone: +1-5124713761.

Author Contributions

[§]These authors contributed equally to this work

Notes

The authors declare no competing financial interest.

■ ACKNOWLEDGMENTS

The authors gratefully acknowledge the U.S. Department of Energy SISGR (DE-FG02-09ER16119) and the Robert A. Welch Foundation (F-0021).

■ REFERENCES

(1) Etgar, L.; Gao, P.; Xue, Z.; Peng, Q.; Chandiran, A. K.; Liu, B.; Nazeeruddin, M. K.; Grätzel, M. Mesoscopic CH3NH3PbI3/TiO2 Heterojunction Solar Cells. *J. Am. Chem. Soc.* **2012**, *134*, 17396−17399.

(2) Kagan, C.; Mitzi, D.; Dimitrakopoulos, C. Organic-inorganic hybrid materials as semiconducting channels in thin-film field-effect transistors. *Science* **1999**, *286*, 945−947.

(3) Kojima, A.; Ikegami, M.; Teshima, K.; Miyasaka, T. Highly luminescent lead bromide perovskite nanoparticles synthesized with porous alumina media. *Chem. Lett.* **2012**, *41*, 397−399.

(4) Gao, P.; Gratzel, M.; Nazeeruddin, M. K. Organohalide lead perovskites for photovoltaic applications. *Energy Environ. Sci.* **2014**, *7*, 2448−2463.

(5) Lee, M. M.; Teuscher, J.; Miyasaka, T.; Murakami, T. N.; Snaith, H. J. Efficient hybrid solar cells based on meso-superstructured organometal halide perovskites. *Science* **2012**, *338*, 643−647.

(6) Burschka, J.; Pellet, N.; Moon, S.-J.; Humphry-Baker, R.; Gao, P.; Nazeeruddin, M. K.; Grätzel, M. Sequential deposition as a route to high-performance perovskite-sensitized solar cells. *Nature* **2013**, *499*, 316−319.

(7) Dou, L.; Yang, Y. M.; You, J.; Hong, Z.; Chang, W.-H.; Li, G.; Yang, Y. Solution-processed hybrid perovskite photodetectors with high detectivity. *Nat. Commun.* **2014**, *5*, 5404.

(8) Zhou, H.; Chen, Q.; Li, G.; Luo, S.; Song, T.-b.; Duan, H.-S.; Hong, Z.; You, J.; Liu, Y.; Yang, Y. Interface engineering of highly efficient perovskite solar cells. *Science* **2014**, *345*, 542−546.

(9) Kojima, A.; Teshima, K.; Shirai, Y.; Miyasaka, T. Organometal halide perovskites as visible-light sensitizers for photovoltaic cells. *J. Am. Chem. Soc.* **2009**, *131*, 6050−6051.

(10) Richard, C. A.; Pan, Z.; Hsu, H.-Y.; Cekli, S.; Schanze, K. S.; Reynolds, J. R. Effect of Isomerism and Chain Length on Electronic Structure, Photophysics, and Sensitizer Efficiency in Quadrupolar (Donor) 2−Acceptor Systems for Application in Dye-Sensitized Solar Cells. *ACS Appl. Mater. Interfaces* **2014**, *6*, 5221−5227.

(11) Nie, W.; Tsai, H.; Asadpour, R.; Blancon, J.-C.; Neukirch, A. J.; Gupta, G.; Crochet, J. J.; Chhowalla, M.; Tretiak, S.; Alam, M. A. High-efficiency solution-processed perovskite solar cells with millimeter-scale grains. *Science* **2015**, *347*, 522−525.

(12) Docampo, P.; Ball, J. M.; Darwich, M.; Eperon, G. E.; Snaith, H. J. Efficient organometal trihalide perovskite planar-heterojunction solar cells on flexible polymer substrates. *Nat. Commun.* **2013**, *4*, 1−6.

(13) Jeon, N. J.; Noh, J. H.; Kim, Y. C.; Yang, W. S.; Ryu, S.; Seok, S. I. Solvent engineering for high-performance inorganic−organic hybrid perovskite solar cells. *Nat. Mater.* **2014**, *13*, 897−903.

(14) McMeekin, D. P.; Sadoughi, G.; Rehman, W.; Eperon, G. E.; Saliba, M.; Hörantner, M. T.; Haghighirad, A.; Sakai, N.; Korte, L.; Rech, B. A mixed-cation lead mixed-halide perovskite absorber for tandem solar cells. *Science* **2016**, *351*, 151−155.

(15) Chen, Z.; Hsu, H.-Y.; Arca, M.; Schanze, K. S. Triplet Energy Transport in Platinum-Acetylide Light Harvesting Arrays. *J. Phys. Chem. B* **2014**, *119*, 7198.

(16) Constantinou, I.; Lai, T. H.; Hsu, H. Y.; Cheung, S. H.; Klump, E. D.; Schanze, K. S.; So, S. K.; So, F. Effect of Thermal Annealing on Charge Transfer States and Charge Trapping in PCDTBT: PC70BM Solar Cells. *Adv. Electron. Mater.* **2015**, *1*, 1500167.

(17) Hartel, M.; Chen, S.; Swerdlow, B.; Hsu, H.-Y.; Manders, J.; Schanze, K.; So, F. Defect-induced loss mechanisms in polymer−inorganic planar heterojunction solar cells. *ACS Appl. Mater. Interfaces* **2013**, *5*, 7215−7218.

(18) Hsu, H.-Y.; Ji, L.; Ahn, H. S.; Zhao, J.; Yu, E. T.; Bard, A. J. A Liquid Junction Photoelectrochemical Solar Cell Based on p-Type MeNH3PbI3 Perovskite with 1.05 V Open-Circuit Photovoltage. *J. Am. Chem. Soc.* **2015**, *137*, 14758−14764.

(19) Niu, G.; Guo, X.; Wang, L. Review of recent progress in chemical stability of perovskite solar cells. *J. Mater. Chem. A* **2015**, *3*, 8970−8980.

(20) Supasai, T.; Rujisamphan, N.; Ullrich, K.; Chemseddine, A.; Dittrich, T. Formation of a passivating CH3NH3PbI3/PbI2 interface during moderate heating of CH3NH3PbI3 layers. *Appl. Phys. Lett.* **2013**, *103*, 183906.

(21) Wang, L.; McCleese, C.; Kovalsky, A.; Zhao, Y.; Burda, C. Femtosecond Time-Resolved Transient Absorption Spectroscopy of

DOI: 10.1021/acs.jpcc.6b07850
J. Phys. Chem. C 2016, 120, 19890−19895

CH3NH3PbI3 Perovskite Films: Evidence for Passivation Effect of PbI2. *J. Am. Chem. Soc.* **2014**, *136*, 12205−12208.
(22) Chen, Q.; Zhou, H.; Song, T.-B.; Luo, S.; Hong, Z.; Duan, H.-S.; Dou, L.; Liu, Y.; Yang, Y. Controllable self-induced passivation of hybrid lead iodide perovskites toward high performance solar cells. *Nano Lett.* **2014**, *14*, 4158−4163.
(23) Im, J.-H.; Lee, C.-R.; Lee, J.-W.; Park, S.-W.; Park, N.-G. 6.5% efficient perovskite quantum-dot-sensitized solar cell. *Nanoscale* **2011**, *3*, 4088−4093.
(24) Zhao, Y.; Zhu, K. CH3NH3Cl-Assisted One-Step Solution Growth of CH3NH3PbI3: Structure, Charge-Carrier Dynamics, and Photovoltaic Properties of Perovskite Solar Cells. *J. Phys. Chem. C* **2014**, *118*, 9412−9418.
(25) Lee, J.; Ye, H.; Pan, S.; Bard, A. J. Screening of photocatalysts by scanning electrochemical microscopy. *Anal. Chem.* **2008**, *80*, 7445−7450.
(26) Fernández, J. L.; Mano, N.; Heller, A.; Bard, A. J. Optimization Of "Wired" Enzyme O2-Electroreduction Catalyst Compositions by Scanning Electrochemical Microscopy. *Angew. Chem.* **2004**, *116*, 6515−6517.
(27) Fernández, J. L.; Mano, N.; Heller, A.; Bard, A. J. Optimization Of "Wired" Enzyme O2-Electroreduction Catalyst Compositions by Scanning Electrochemical Microscopy. *Angew. Chem., Int. Ed.* **2004**, *43*, 6355−6357.
(28) Mano, N.; Kim, H.-H.; Heller, A. On the relationship between the characteristics of bilirubin oxidases and O2 cathodes based on their "wiring. *J. Phys. Chem. B* **2002**, *106*, 8842−8848.
(29) Leonard, K. C.; Nam, K. M.; Lee, H. C.; Kang, S. H.; Park, H. S.; Bard, A. J. ZnWO4/WO3 composite for improving photoelectrochemical water oxidation. *J. Phys. Chem. C* **2013**, *117*, 15901−15910.
(30) Stoumpos, C. C.; Malliakas, C. D.; Kanatzidis, M. G. Semiconducting tin and lead iodide perovskites with organic cations: phase transitions, high mobilities, and near-infrared photoluminescent properties. *Inorg. Chem.* **2013**, *52*, 9019−9038.
(31) Cao, D. H.; Stoumpos, C. C.; Malliakas, C. D.; Katz, M. J.; Farha, O. K.; Hupp, J. T.; Kanatzidis, M. G. Remnant PbI2, an unforeseen necessity in high-efficiency hybrid perovskite-based solar cells? a). *APL Mater.* **2014**, *2*, 091101.
(32) Stranks, S. D.; Eperon, G. E.; Grancini, G.; Menelaou, C.; Alcocer, M. J.; Leijtens, T.; Herz, L. M.; Petrozza, A.; Snaith, H. J. Electron-hole diffusion lengths exceeding 1 micrometer in an organometal trihalide perovskite absorber. *Science* **2013**, *342*, 341−344.
(33) Pellet, N.; Gao, P.; Gregori, G.; Yang, T. Y.; Nazeeruddin, M. K.; Maier, J.; Grätzel, M. Mixed-organic-cation Perovskite photovoltaics for enhanced solar-light harvesting. *Angew. Chem., Int. Ed.* **2014**, *53*, 3151−3157.
(34) Ponseca, C. S.; Savenije, T. J.; Abdellah, M.; Zheng, K.; Yartsev, A.; Pascher, T.; Harlang, T.; Chabera, P.; Pullerits, T.; Stepanov, A.; Wolf, J.-P.; Sundström, V. Organometal Halide Perovskite Solar Cell Materials Rationalized: Ultrafast Charge Generation, High and Microsecond-Long Balanced Mobilities, and Slow Recombination. *J. Am. Chem. Soc.* **2014**, *136*, 5189−5192.
(35) Sum, T. C.; Mathews, N. Advancements in perovskite solar cells: photophysics behind the photovoltaics. *Energy Environ. Sci.* **2014**, *7*, 2518−2534.
(36) Song, D.; Cui, P.; Wang, T.; Wei, D.; Li, M.; Cao, F.; Yue, X.; Fu, P.; Li, Y.; He, Y.; Jiang, B.; Trevor, M. Managing Carrier Lifetime and Doping Property of Lead Halide Perovskite by Postannealing Processes for Highly Efficient Perovskite Solar Cells. *J. Phys. Chem. C* **2015**, *119*, 22812−22819.
(37) Xing, G.; Mathews, N.; Sun, S.; Lim, S. S.; Lam, Y. M.; Grätzel, M.; Mhaisalkar, S.; Sum, T. C. Long-range balanced electron-and hole-transport lengths in organic-inorganic CH3NH3PbI3. *Science* **2013**, *342*, 344−347.
(38) Hsu, H.-Y.; Vella, J. H.; Myers, J. D.; Xue, J.; Schanze, K. S. Triplet Exciton Diffusion in Platinum Polyyne Films. *J. Phys. Chem. C* **2014**, *118*, 24282−24289.

DOI: 10.1021/acs.jpcc.6b07850
J. Phys. Chem. C 2016, 120, 19890−19895